BOLETIN DE LA SOCIEDAD ESPAÑOLA DE
Cerámica y Vidrio
www.elsevier.es/bsecv

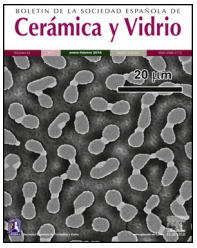

Nucleation and growth of brushite crystals on the graphene sheets applicable in bone cement

Hassan Nosrati[a,*], *Dang Quang Svend Le*[b], *Reza Zolfaghari Emamehc*[c], *Maria Canillas Perez*[d], *Cody Eric Bünger*[b]

[a] *Department of Materials Engineering, Tarbiat Modares University, Tehran, Iran*
[b] *Department of Clinical Medicine, Aarhus University, Denmark*
[c] *Department of Energy and Environmental Biotechnology, National Institute of Genetic Engineering and Biotechnology (NIGEB), Tehran, Iran*
[d] *Instituto de Cerámica y Vidrio, CSIC, Madrid, Spain*

ARTICLE INFO

Article history:
Received 17 February 2020
Accepted 5 May 2020
Available online 30 May 2020

Keywords:
Graphene oxide
Brushite
Setting time
Modeling
Bone cement

ABSTRACT

Since recent research indicates that the addition of graphene increases the mechanical and biological properties of calcium phosphates simultaneously, graphene oxide (GO) was used in this research to enhance the properties of brushite cement. The main objective of this study is to investigate the mechanism of nucleation and growth of brushite crystals on GO sheets. Calcium nitrate tetrahydrate and diammonium hydrogenphosphate were used as calcium and phosphate precursors. The brushite chemical precipitation method on graphene sheets was used in this study and computer-assisted modeling was used to understand the process. The results of this study showed that the hybrid powders contained brushite and GO. Brushite crystals were grown after nucleation in proportion to the three main planes containing (020), (12$\bar{1}$), and (141). The final particles were plate shaped. The results of setting time tests showed that increasing the GO% decreases the setting time and this trend continues with an increasing amount of GO. The results of the mechanical evaluation showed that increasing the GO by up to 2% increased the mechanical properties and more than that decreased the mechanical properties.

Nucleación y crecimiento de cristales de brushita sobre láminas de grafeno para su aplicación como cementos óseos

Palabras clave:
Oxido de grafeno
Brushita

RESUMEN

Estudios recientes muestran una mejora de las propiedades mecánicas y biológicas de los fosfatos de calcio con la adición de grafeno. En este trabajo, el óxido de grafeno (GO) se propone para mejorar las propiedades de cementos de composición brushita. El

* *Corresponding author.*
E-mail address: h.nosrati@modares.ac.ir (H. Nosrati).
https://doi.org/10.1016/j.bsecv.2020.05.001

Tiempo de endurecimiento
Modelado
Cemento para defectos óseos

principal objetivo es estudiar el mecanismo de nucleación de cristales de brushita sobre láminas de grafeno. Como precursores de calcio y fosfato se han usado nitrato cálcico tetrahidratado e hidrogenofosfato amónico. Para comprender el proceso se ha usado el método de precipitación química de la brushita sobre láminas de grafeno, y la modelización asistida por ordenador. Los resultados mostraron que el producto de síntesis consistía en un polvo híbrido que contenía brushita y GO. Los cristales de brushita crecieron, tras su nucleación, a lo largo de los planos principales (020), (12$\bar{1}$) y (141). Las partículas resultantes tienen morfología de plaquetas. Las medidas de los tiempos de endurecimiento mostraron que el aumento en GO disminuye el tiempo de endurecimiento. En cuanto al estudio de las propiedades mecánicas reveló que el incremento en GO, hasta del 2%, mejora las propiedades mecánicas para disminuir una vez se excede dicha cantidad.

Introduction

Millions of patients are hospitalized every year because of bone defects caused by skeletal diseases, congenital anomalies, traumatic events, and malignancies. For the past two centuries, bone marrow transplants have been performed on patients using their own (autograft) or another (allograft) organ. However, problems such as poisoning of donor sites, access restrictions, and increased procedural costs have led to increased research on replacement biomaterials [1–3]. Of all the materials that were nominated for the study, the calcium phosphate family attracted most of the researchers' attention. The reason for this was the unique properties of these materials, which include non-immunogenicity, osteoconductivity, biocompatibility, non-toxicity, and bioactivity [4–6]. Calcium phosphate family such as hydroxyapatite, tetra calcium phosphate, α-tricalcium phosphate (α-TCP), β-tricalcium phosphate (β-TCP), dicalcium phosphate dehydrate, decalcium phosphate anhydrous, octa calcium phosphate, and so on, have been used in a variety of applications such as bone cement, coating, and orthopedics [7,8]. These materials are injectable and harden by combining crystals with needle and plate forms in situ [9,10].

One important point is that the amount of calcium phosphate in the resin phase (such as di- or triethylene glycol dimethacrylate as a matrix in resin-based composite) should be low to avoid stress concentration, as well as not to alter alkaline conditions (pH > 7) [11,12]. Recent researches have shown that the biodegradability of dicalcium phosphate dehydrate (DCPD, brushite) in the body is higher than that of hydroxyapatite, and due to its potential to become dicalcium phosphate anhydrous (DCPA, monetite), it exhibits remarkable osteoconductive and osteoinductive properties [13]. Brushite also has other properties that are superior to those of other calcium phosphate members for bone cement applications, which include rapid replacement of bone tissue, better refractive index, and less expensive. But like other calcium phosphates it has poor mechanical properties and needs to be improved for use in regenerative medicine through reinforcement additives [14–16].

Many studies have been done in the past few years on carbon nanomaterials especially graphene and GO. This material has received much attention in orthopedic applications because of their good biocompatibility properties [17–19]. These materials have excellent mechanical properties and their two-dimensional structure has made them highly reinforcing [20]. Particularly, GO is very suitable for the synthesis of hybrid materials by chemical methods such as hydrothermal process and precipitation method due to the presence of surface agents. Also, GO is hydrophilic and is well dispersed in most solvents such as N-methylpyrrolidinone (NMP), tetrahydrofuran (THF), dimethylformamide (DMF), and deionized water. GO can recover most of the properties of graphene sheets through its heat, light, or chemical reduction [21–24]. Chemical precipitation of calcium phosphates on GO is accomplished by stirring GO into the solvent to homogenize the solution. Then the solution containing calcium ions (calcium carbonate/hydroxide/calcium nitrate) is added and stirred again to bind to the GO surface agents by Van der Waals forces. Finally, the solution containing phosphate ions (hydrogen phosphate diammonium/phosphoric acid) is added to the previous set and adjusted its pH to control the product morphology and type [25–29].

Since recent research indicates that the addition of graphene sheets increases the mechanical and biological properties of calcium phosphates simultaneously [30–33], GO was used in this research to enhance the properties of brushite. The main objective of this study is to investigate the mechanism of nucleation and growth of brushite crystals on GO sheets. For this purpose, computer aided drawn models, according to existing standards, have been assisted for structural study. In this study, the type of precursors, their ratios, and control factors were determined according to previous studies [34,35]. To investigate the use of these powders in bone cement, a combination of powders synthesized with different GO% with β-TCP purchased was prepared as a composite and their compression strength and setting time were evaluated.

Experimental

The chemicals used in this study include calcium nitrate tetrahydrate (Merck, >99%, $Ca(NO_3)_2{\cdot}4H_2O$), diammonium hydrogenphosphate (Merck, >99%, $(NH_4)_2HPO_4$), diethylene glycol (DEG, Sigma Aldrich, 99%, $(HOCH_2CH_2)_2O$), ammonium solution (Merck, 25%, NH_4OH), and anhydrous ethanol (Sigma

Table 1 – Characterization methods.

Characterization method	Device specifications
X-ray diffraction (XRD)	X' Pert Pro, Panalytical Co., Cu Kα radiation, λ = 1.5406 Å, 40 kV, 40 mA, 2θ scanning range from 10° up to 60° in steps of 0.02°
Fourier transform infrared spectroscopy (FTIR)	VERTEX 70, Bruker Corp., resolution of 4 cm^{-1}, scan number of 8, 200 MPa pressures, and room conditions (25 °C, 60% relative humidity), spectral region from 400 to 4000 cm^{-1} using 2 cm^{-1} steps
Micro-Raman spectroscopy	Renishaw inVia spectrometer, wavelength of 532 nm, green laser line (argon ion laser) in a backscattering configuration, range of 300–3500 cm^{-1}, recording 5 times for 10 s of each accumulation
Field Emission Scanning Electron Microscope (FESEM)	Hitachi S4700 equipped with energy dispersive X-ray spectroscopy, the samples mounted in an adhesive carbon film, Au coated by sputtering
Inductively Coupled Plasma (ICP)	DV7300, Optima Co
Transmittance Electron Microscopy (TEM)	CM120, Philips
X-ray Photoelectron Spectroscopy (XPS)	XPS, Thermo ESCALAB 250XI

Aldrich, >99%, CH_3CH_2OH), β-TCP powders (Puriss. P.a, >98%, $Ca_3O_8P_2$), disodium dihydrogen pyrophosphate (SPP, Sigma Aldrich). GO was prepared by oxidation and exfoliation of graphite via the modifed Hummer's method [36].

Preparation of samples

Stoichiometric amount of calcium nitrate tetrahydrate and diammonium hydrogenphosphate were dissolved in anhydrous ethanol and deionized water, respectively. First, the solution containing calcium ions was added dropwise to a 20 mL suspension of GO in DEG (The ratio of chemicals used was calculated to finally obtain four types of powders with 0%, 1.82%, 3.64%, and 5.45% GO, by weight), which was stirring, and continued for an hour. Then, the solution containing phosphate ions was added dropwise to the previous set and finally the pH of the solutions was adjusted with ammonium solution. The precipitate was centrifuged, washed with deionized water and anhydrous ethanol several times, and then dried in a vacuum oven at 80 °C for 12 h. To examine the powders characteristics and their application, the powders with the highest amount of GO (5.45%) were first evaluated as a representative of all powders. Then, to investigate the effect of this type of powders on bone cement applications, all four types of powders were mixed with β-TCP with a ratio of 45:55 (by weight), so that the resulting bone cement composite would contain 0%, 1%, 2%, and 3% GO.

Characterization

The characterization methods used in this study with the specifications are listed in Table 1 [37]. ImageJ 1.52d and Diamond 3.2 softwares were used in this study.

Setting time and compression testing

Bone cement was first prepared for time setting test and compression testing. The method of samples preparation and chemical additives required was performed in accordance with the previously published method and the standards listed therein [38]. For this purpose, the powders synthesized in this study were mixed with β-TCP powders at a ratio of 55:45.

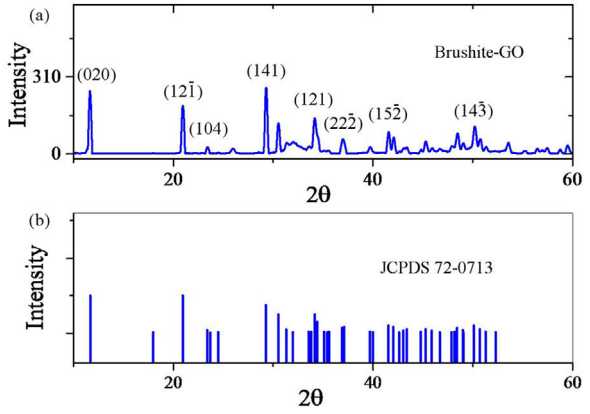

Fig. 1 – (a) XRD analysis of brushite-GO powders (5.45% GO), (b) JCPDS 72-0713 standard.

The ratio of GO in the initial precipitation section was taken into account in the final samples with 0, 1, 2, and 3% GO. The cement pastes were placed in a Teflon mold (diameter of 6 mm, height of 12 mm) and set in a 100% relative humidity box at 37 °C. Setting times were measured by employing the Vicat needle (ASTM C187-98). After setting for 24 h at 37 °C and drying at 70 °C overnight, the compressive strength of composites was measured under loading rate of 1 mm/min (with a universal testing machine, STM 20).

Results and discussion

To characterize the powders, brushite-5.45%GO powder was used and brushite-GO was used to simplify the discussion. Therefore, in all analyzes, brushite-GO means brushite-5.45%GO. Fig. 1 shows the XRD pattern of the synthesized powders and the standard for pure brushite (JCPDS 72-0713). These two patterns are very similar; therefore, it can be argued that the synthesized calcium phosphate is brushite having a monoclinic structure. The pattern of the synthesized powders containing GO, shows only brushite phase [39–41]. The GO peaks in this spectrum are probably overlapped with the brushite peaks and therefore more analysis (Raman

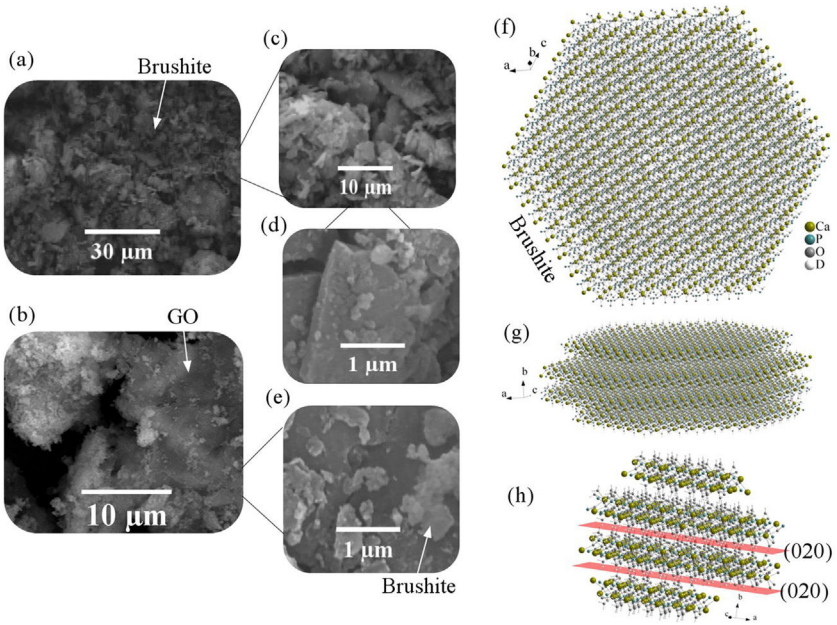

Fig. 2 – (a–e) FESEM images of brushite-GO powders (5.45% GO), (f–h) Computer assisted models in two directions.

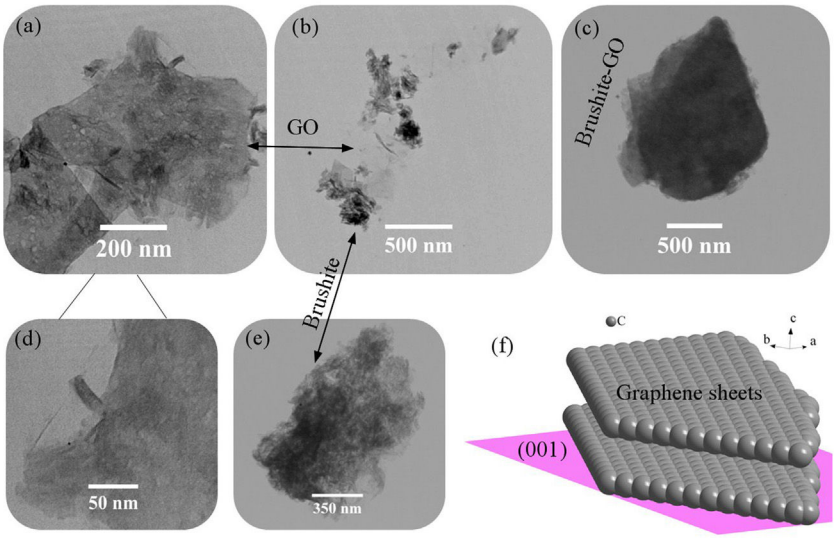

Fig. 3 – (a–e) TEM images of brushite-GO powders (5.45% GO), (f) (001) plane of GO.

spectroscopy, TEM) is needed to prove the existence of GO sheets. As the crystals grow, some of these planes are preferable to the others and show a higher intensity in the XRD pattern [42–44].

Schematic 1 shows the preferred crystal growth planes. When the crystal starts to grow, crystal growth takes place in all three main directions. But in the following, the combination of growth directions continues and by blocking in some ways, eventually the particles form flat polygons. The rate of growth varies in different directions, so over time, the particles morphology goes out of symmetry. Also, in the interfaces between graphene sheets and brushite particles, the particles growth stops. The specification applied to the modeling is according to the d-spacing of the planes obtained from XRD analysis. The distance between these planes and the distance between the carbon atoms in the GO structure plays a crucial role in the interface of the two phases, and the orientation of brushite particles and GO sheets relative to each other.

Fig. 2 shows the FESEM images of brushite-GO powders and computer assisted models in two directions. The particles shape is like polygon plates and asymmetric. The plates dimensions are in micrometers. If the powders' images (Fig. 2a–e) are compared to those of the drawn models (Fig. 2f–h), the (020) planes are tangent to the plate surface and that means there has been growth restriction in this direction (the authors' hypothesis). Spherical particles are probably due to GO sheets that are folded up [45].

Fig. 3 shows the TEM images of brushite-GO powders and the schematic image of GO (001) plane. Fig. 3a–d shows the presence of GO sheets, which are composed of brushite

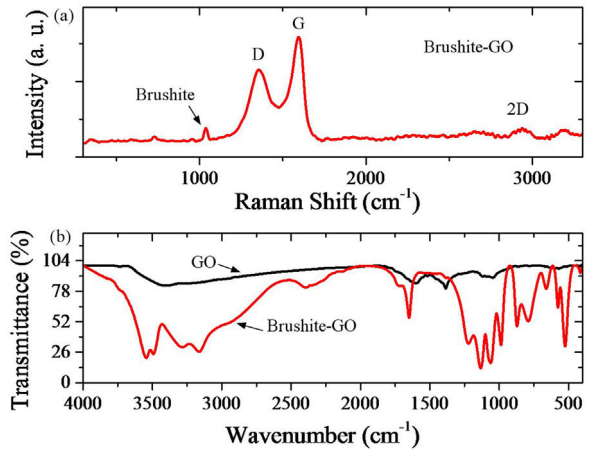

Fig. 4 – (a) Raman spectrum of brushite-GO powders (5.45% GO), (b) FTIR analysis of GO and brushite-GO powders (5.45% GO).

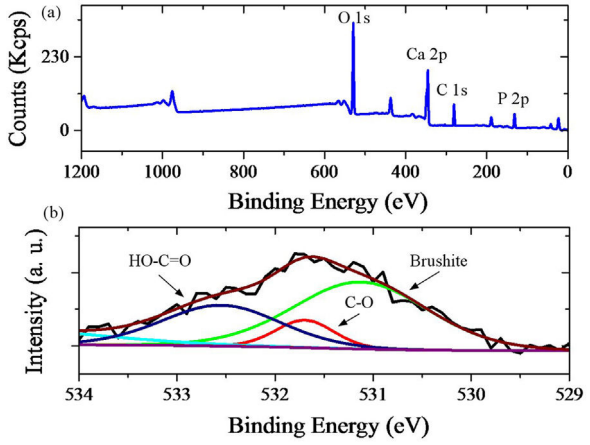

Fig. 5 – (a) XPS analysis of brushite-GO powders (5.45% GO), (b) high resolution fitted curves.

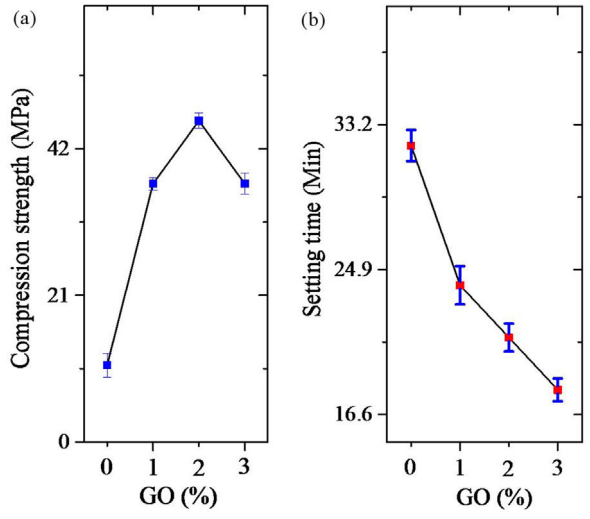

Fig. 6 – (a) Compression strength of cement samples, (b) setting time of cement samples.

particles on its surface and at its edges. Fig. 3e shows the brushite constituent particles that are convex in shape and dense. Fig. 3f shows that the GO (001) planes and edges are suitable sites for brushite growth. The agents present on the GO surface and its edges attach to the brushite particles by Van der Waals bond (the authors' hypothesis).

Fig. 4 shows the Raman spectrum of brushite-GO powders, and FTIR analysis of GO and brushite-GO powders. Regarding the Raman spectroscopy result (Fig. 4a), the main bonds in the spectrum are the phosphate bonds. Brushite Raman vibrations are associated with different modes of internal tetragonal states. The peak located at 1060 cm^{-1} is corresponding to a totally symmetric stretching mode of the tetrahedral PO_4^{3-} group (P—O bond) and the peak located at 750 cm^{-1} is related to a doubly degenerate bending mode of the phosphate group (P—O—P bond). All three shifts obtained in D (located at 1350 cm^{-1}, related to the carbon atoms A1 g symmetric oscillations of with the sp^3 hybrid in GO), G (located at 1600 cm^{-1}, related to the shaking of the carbon atoms phonon's E2 g with the sp^2 hybrid in GO), and 2D (located at 2700 cm^{-1}, 2D peak is related to the number of layers of GO) are related to carbon compounds such as GO. These peaks along with previous microscopic images are the best evidence of the presence of GO compounds in the synthesized powders. Regarding the FTIR result (Fig. 4b), the wide peaks between 2500 cm^{-1} and 3500 cm^{-1} are related to the O—H band stretching vibrations. The peak located at 1650 cm^{-1} is due to H—O—H bending and the peaks located at 1065 cm^{-1}, 1130 cm^{-1} and 1215 cm^{-1} are related to O=P bands stretching vibrations. The peaks located at 980 cm^{-1}, 870 cm^{-1} and 790 cm^{-1} are related to the P—O—P asymmetric stretching vibrations. The peaks located in 525 cm^{-1} and 580 cm^{-1} are due to (H—O—) bonds. Due to the presence of graphene oxide, the peaks associated with GO and the peaks associated with the brushite are likely to be overlapping. Some GO peaks in brushite-GO powders have been moved slightly upwards due to a small amount of reduction in GO [42–44].

Fig. 5 shows the XPS analysis of brushite-GO powders, and high resolution fitted curves. GO spectrum should contain carbon (284–289 eV) and oxygen. Ca 2p and P 2p peaks are characteristics of brushite and can confirm the synthesis of this phase (Fig. 5a). The high resolution XPS spectrum of O 1s of the brushite-GO powders is shown in Fig. 5b, in which the peak centered at 531 eV is attributed to the oxygen in brushite and OH groups, whereas those at 533 and 532 eV correspond to the oxygen in C—O and H—C=O groups (GO). The XPS results further reveal the presence of brushite and GO, which agree with the Raman spectroscopy results [46,47].

Schematic 2 shows the brushite nucleation mechanism and brushite-GO interfaces after growth (the authors' hypothesis). According to this model, calcium ions are first attracted by Van der Waals forces to the GO surface agents and edges. Subsequently, phosphate ions bond with calcium ions and early nuclei are formed (Schematic 2a). The spacing between the (001) planes in GO is about 0.8 nm, which corresponds to the d-spacing of (020) planes in the brushite (0.76 nm). Therefore, the relationship between the two phases at the edge of the sheets and at the surface will be as Schematic 2b. The amount of GO does not have much effect on the growth of brushite crystals, because growth happens on both sides and

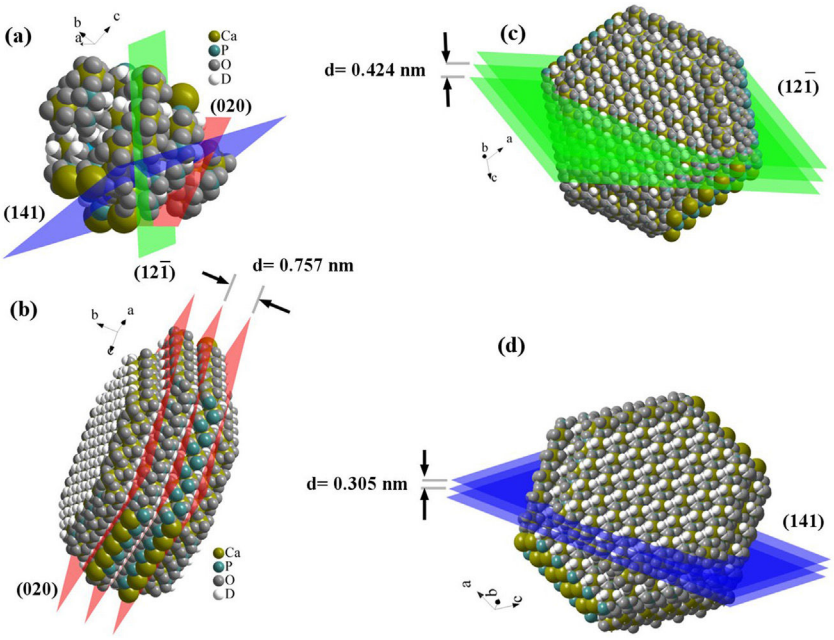

Schematic 1 – (a) Brushite crystal nucleation, (b) growth by (020) planes, (c) growth by.

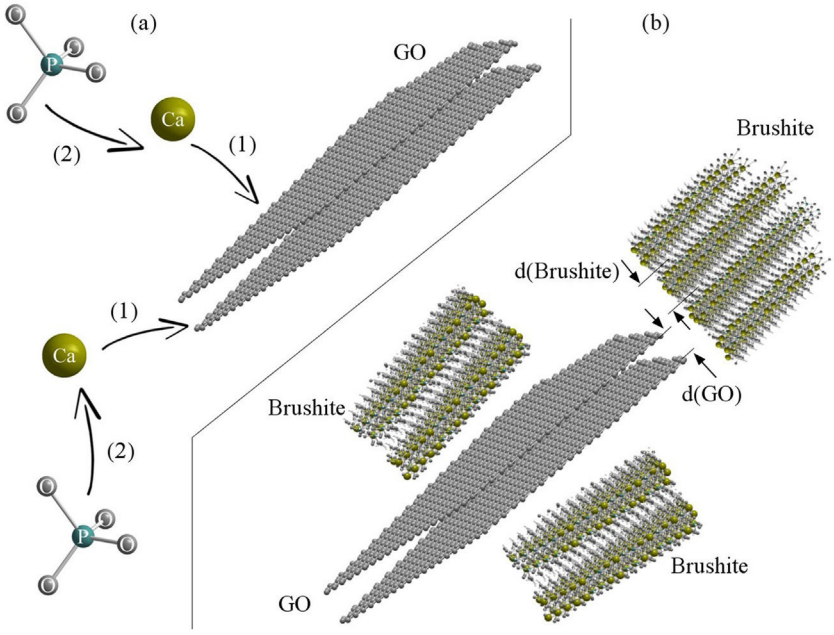

Schematic 2 – (a) Nucleation mechanism, (b) brushite-GO interfaces after growth.

when one side is limited, it continues on the other side. Also, planes bounded by GO contribute less to the growth of crystals [42–44].

Fig. 6 shows the results of compression testing, and setting time of cements. As is evident (Fig. 6a), by increasing the amount of GO to 2%, the compressive strength of the cement increases but decreases thereafter. Increasing the amount of GO is likely to cause the cavities between the folded GO sheets to become larger than necessary and reduce the strength. But as the amount of GO increases, the setting time decreases continuously. These findings show that the optimum amount of GO is 2% by weight.

Based on the results of studies on bone cements and calcium phosphates, the findings of this research have the potential to be used in a wide range of applications. The use of these powders made the setting time obtained competitive with other works. Due to the simplicity of the synthesis of these powders, and the significant effect of graphene sheets on increasing the mechanical behavior of bone cements, these

types of powders can create a new paradigm in the treatment of bone diseases [48–50].

Conclusions

The results of this study showed that the synthesized powders contained brushite and GO. Brushite crystals were grown after nucleation in proportion to the three main planes containing (020), (12$\bar{1}$), and (141) independent of %GO. The final particles were plate shaped. The results of setting time tests showed that increasing the GO decreased the setting time and this trend continued with increasing amount of GO. The results of the mechanical evaluation showed that increasing the GO by up to 2% increased the mechanical properties and more than that decreased the mechanical properties in bone cement application.

Conflict of interests

The Authors declare that there is no conflict of interest.

REFERENCES

[1] J. Zhang, W. Liu, V. Schnitzler, F. Tancret, J.M. Bouler, Calcium phosphate cements for bone substitution: chemistry, handling and mechanical properties, Acta Biomater. 10 (3) (2014) 1035–1049, http://dx.doi.org/10.1016/j.actbio.2013.11.001.

[2] Y. Xia, H. Chen, F. Zhang, C. Bao, M.D. Weir, M.A. Reynolds, J. Ma, N. Gu, H.H.K. Xu, Gold nanoparticles in injectable calcium phosphate cement enhance osteogenic differentiation of human dental pulp stem cells, Nanomed. Nanotechnol. Biol. Med. 14 (1) (2018) 35–45, http://dx.doi.org/10.1016/j.nano.2017.08.014.

[3] Z. Sheikh, Y.L. Zhang, F. Tamimi, J. Barralet, Effect of processing conditions of dicalcium phosphate cements on graft resorption and bone formation, Acta Biomater. 53 (2017) 526–535, http://dx.doi.org/10.1016/j.actbio.2017.02.022.

[4] A.H. Ahmadi, H. Nosrati, R. Sarraf-Mamoory, Decreasing β-three calcium phosphate particle size using graphite as nucleation sites and diethylene glycol as a chemical additive, J. Bioeng. Res. 1 (4) (2019) 50–59, http://dx.doi.org/10.22034/JBR.2019.211371.1016.

[5] A. Topsakal, M. Uzun, G. Ugar, A. Ozkan, E. Altun, F.N. Oktar, F. Ikram, O. Ozkan, H.T. Sasmazel, O. Gunduz, Development of amoxicillin loaded electrospun polyurethane/chitosan/β-tricalcium phosphate scaffold for bone tissue regeneration, IEEE Trans. NanoBiosci. 17 (3) (2018) 321–328, http://dx.doi.org/10.1109/TNB.

[6] H. Nosrati, D.Q.S. Le, R.Z. Emameh, C.E. Bünger, Characterization of the precipitated dicalcium phosphate dehydrate on the graphene oxide surface as a bone cements reinforcement, J. Tissues Mater. 2 (1) (2019) 33–46, http://dx.doi.org/10.22034/jtm.2019.173565.1013.

[7] M. Canillas, P. Pena, A.H. de Aza, M.A. Rodríguez, Calcium phosphates for biomedical applications, boletín de la sociedad española de cerámica y vidrio, vol. 56, 2017, pp. 91–112, http://dx.doi.org/10.1016/j.bsecv.2017.05.001.

[8] X. Li, Z. Weng, W. Yuan, X. Luo, H.M. Wong, X. Liu, S. Wu, K.W.K. Yeung, Y. Zheng, P.K. Chu, Corrosion resistance of dicalcium phosphatedihydrate/poly (lactic-co-glycolic acid) hybrid coating on AZ31 magnesium alloy, Corros. Sci. 102 (2016) 209–221, http://dx.doi.org/10.1016/j.corsci.2015.10.010.

[9] H.H.K. Xu, P. Wang, L. Wang, C. Bao, Q. Chen, M.D. Weir, L.C. Chow, L. Zhao, X. Zhou, M.A. Reynolds, Calcium phosphate cements for bone engineering and their biological properties, Bone Res. 5 (2017) 17056, http://dx.doi.org/10.1038/boneres.2017.56.

[10] C.L. Ko, J.C. Chen, C.C. Hung, J.C. Wang, Y.C. Tien, W.C. Chen, Biphasic products of dicalcium phosphate-rich cement with injectability and nondispersibility, Mater. Sci. Eng. C 39 (2014) 40–46, http://dx.doi.org/10.1016/j.msec.2014.02.033.

[11] L.C. Natale, M.C. Rodrigues, Y. Alania, M.D.S. Chiari, L.C.C. Boaro, M. Cotrim, O. Vega, R.R. Braga, Mechanical characterization and ion release of bioactive dental composites containing calcium phosphate particles, J. Mech. Behav. Biomed. Mater. 84 (2018) 161–167, http://dx.doi.org/10.1016/j.jmbbm.2018.05.022.

[12] M.D.S. Chiari, M.C. Rodrigues, T.A. Xavier, E.M.N. de Souza, V.E. Arana-Chavez, R.R. Braga, Mechanical properties and ion release frombioactive restorative composites containing glassfillers and calcium phosphate nano-structured particles, Dental Mater. 31 (2015) 726–733, http://dx.doi.org/10.1016/j.dental.2015.03.015.

[13] Z. Sheikh, Y.L. Zhang, L. Grover, G.E. Merle, F. Tamimi, J. Barralet, In vitro degradation and in vivo resorption of dicalcium phosphate cement based grafts, Acta Biomater. 26 (2015) 338–346, http://dx.doi.org/10.1016/j.actbio.2015.08.031.

[14] F. Tamimi, D. Le Nihouannen, H. Eimar, Z. Sheikh, S. Komarova, J. Barralet, The effect of autoclaving on the physical and biological properties of dicalcium phosphate dihydrate bioceramics: brushite vs. monetite, Acta Biomater. 8 (2012) 3161–3169, http://dx.doi.org/10.1016/j.actbio.2012.04.025.

[15] D. Kajánek, F. Pastorek, S. Fintová, A. Bača, Study of corrosion behavior of dicalcium phosphate-dihydrate (DCPD) coating prepared by large amplitude sinusoidal voltammetry (LASV) technique on ZW3 magnesium alloy, Proc. Eng. 192 (2017) 399–403, http://dx.doi.org/10.1016/j.proeng.2017.06.069.

[16] I. Ajaxon, A. Acciaioli, G. Lionello, M.P. Ginebra, C. Öhman-Mägi, M. Baleani, C. Persson, Elastic properties and strain-to-crack-initiation of calcium phosphate bone cements: revelations of a high-resolution measurement technique, J. Mech. Behav. Biomed. Mater. 74 (2017) 428–437, http://dx.doi.org/10.1016/j.jmbbm.2017.06.023.

[17] A. Janković, S. Eraković, M. Mitrić, I.Z. Matić, Z.D. Juranić, G.C. Tsui, C.Y. Tang, V. Mišković-Stanković, K.Y. Rhee, S.J. Park, Bioactive hydroxyapatite/graphene composite coating and its corrosion stability in simulated body fluid, J. Alloys Compounds 624 (2014) 148–157, http://dx.doi.org/10.1016/j.jallcom.2014.11.078.

[18] D. Lahiri, S. Ghosh, A. Agarwal, Carbon nanotube reinforced hydroxyapatite composite for orthopedic application: a review, Mater. Sci. Eng. C 32 (7) (2012) 1727–1758, http://dx.doi.org/10.1016/j.msec.2012.05.010.

[19] L. Zhang, W. Liu, C. Yue, T. Zhang, P. Li, Z. Xing, Y. Chen, A tough graphene nanosheet/hydroxyapatite composite with improved in vitro biocompatibility, Carbon 61 (2013) 105–115, http://dx.doi.org/10.1016/j.carbon.2013.04.074.

[20] C. Lee, X. Wei, J.W. Kysar, J. Hone, Measurement of the elastic properties and intrinsic strength of monolayer graphene, science 321 (2008) 385–388, http://dx.doi.org/10.1126/science.1157996.

[21] D.R. Dreyer, S. Park, C.W. Bielawski, R.S. Ruoff, The chemistry of graphene oxide, Chem. Soc. Rev. 39 (1) (2010) 228–240, http://dx.doi.org/10.1039/b917103g.

[22] W. Hu, C. Peng, W. Luo, M. Lv, X. Li, D. Li, Q. Huang, C. Fan, Graphene-based antibacterial paper, ACS Nano 4 (7) (2010) 4317–4323, http://dx.doi.org/10.1021/nn101097v.

[23] J. Kim, L.J. Cote, F. Kim, W. Yuan, K.R. Shull, J. Huang, Graphene oxide sheets at interfaces, J. Am. Chem. Soc. 132 (23) (2010) 8180–8186, http://dx.doi.org/10.1021/ja102777.
[24] Y. Zhu, S. Murali, W. Cai, X. Li, J.W. Suk, J.R. Potts, R.S. Ruoff, Graphene and graphene oxide: synthesis, properties, and applications, Adv. Mater. 22 (35) (2010) 3906–3924, http://dx.doi.org/10.1002/adma.201001068.
[25] M. Li, Y. Wang, Q. Liu, Q. Li, Y. Cheng, Y. Zheng, T. Xi, S. Wei, In situ synthesis and biocompatibility of nano hydroxyapatite on pristine and chitosan functionalized graphene oxide, J. Mater. Chem. B 1 (4) (2013) 475–484, http://dx.doi.org/10.1039/C2TB00053A.
[26] Y. Liu, Z. Dang, Y. Wang, J. Huang, H. Li, Hydroxyapatite/graphene-nanosheet composite coatings deposited by vacuum cold spraying for biomedical applications: Inherited nanostructures and enhanced properties, Carbon 67 (2014) 250–259, http://dx.doi.org/10.1016/j.carbon.2013.09.088.
[27] G.M. Neelgund, A. Oki, Z. Luo, In situ deposition of hydroxyapatite on graphene nanosheets, Mater. Res. Bull. 48 (2) (2013) 175–179, http://dx.doi.org/10.1016/j.materresbull.2012.08.077.
[28] J.D. Núñez, A.M. Benito, R. González, J. Aragón, R. Arenal, W.K. Maser, Integration and bioactivity of hydroxyapatite grown on carbon nanotubes and graphene oxide, Carbon 79 (2014) 590–604, http://dx.doi.org/10.1016/j.carbon.2014.08.020.
[29] A. Oyefusi, O. Olanipekun, G.M. Neelgund, D. Peterson, J.M. Stone, E. Williams, L. Carson, G. Regisford, A. Oki, Hydroxyapatite grafted carbon nanotubes and graphene nanosheets: promising bone implant materials, Spectrochim. Acta A: Mol. Biomol. Spectrosc. 132 (2014) 410–416, http://dx.doi.org/10.1016/j.saa.2014.04.004.
[30] Z. Fan, J. Wang, Z. Wang, H. Ran, Y. Li, L. Niu, P. Gong, B. Liu, S. Yang, One-pot synthesis of graphene/hydroxyapatite nanorod composite for tissue engineering, Carbon 66 (2014) 407–416, http://dx.doi.org/10.1016/j.carbon.2013.09.016.
[31] C. Qi, Y.J. Zhu, G.J. Ding, J. Wu, F. Chen, Solvothermal synthesis of hydroxyapatite nanostructures with various morphologies using adenosine 5′-monophosphate sodium salt as an organic phosphorus source, RSC Adv. 5 (5) (2015) 3792–3798, http://dx.doi.org/10.1039/C4RA13151G.
[32] J.W. Kim, Y.C. Shin, J.J. Lee, E.B. Bae, Y.C. Jeon, C.M. Jeong, M.J. Yun, S.H. Lee, D.W. Han, J.B. Huh, The effect of reduced graphene oxide-coated biphasic calcium phosphate bone graft material on osteogenesis, Int. J. Mol. Sci. 18 (2017) 1725, http://dx.doi.org/10.3390/ijms18081725.
[33] J.J. Lee, Y.C. Shin, S.J. Song, J.M. Cha, S.W. Hong, Y.J. Lim, S.J. Jeong, D.W. Han, B. Kim, Dicalcium phosphate coated with graphene synergistically increases osteogenic differentiation in vitro, Coatings 8 (13) (2018), http://dx.doi.org/10.3390/coatings8010013.
[34] H. Nosrati, R. Sarraf-Mamoory, F. Dabir, Crystallographic study of hydrothermal synthesis of hydroxyapatite nano-rods using Brushite precursors, J. Tissues Mater. 2 (3) (2019) 1–8, http://dx.doi.org/10.22034/jtm.2019.199830.1022.
[35] H. Nosrati, R. Sarraf-Mamoory, D.Q.S. Le, C.E. Bünger, Fabrication of gelatin/hydroxyapatite/3D-graphene scaffolds by a hydrogel 3D-printing method, Mater. Chem. Phys. 239 (2020) 122305, http://dx.doi.org/10.1016/j.matchemphys.2019.122305.
[36] H.N. Lim, N.M. Huang, S.S. Lim, I. Harrison, C.H. Chia, Fabrication and characterization of graphene hydrogel via hydrothermal approach as a scaffold for preliminary study of cell growth, Int. J. Nanomed. 6 (2011) 1817–1823, http://dx.doi.org/10.2147/IJN.S23392.
[37] H. Nosrati, R. Sarraf Mamoory, D.Q.S. Le, C.E. Bünger, R.Z. Emameh, F. Dabir, Gas injection approach for synthesis of hydroxyapatite nanorods via hydrothermal method, Mater. Charact. 159 (2019) 110071, http://dx.doi.org/10.1016/j.matchar.2019.110071.
[38] J. Unosson, H. Engqvist, Development of a resorbable calcium phosphate cement with load bearing capacity, Bioceram. Dev. Appl. 4 (2014) 1–4, http://dx.doi.org/10.4172/2090-5025.1000074.
[39] H. Nosrati, R. Sarraf Mamoory, F. Dabir, M.C. Perez, M.A. Rodriguez, D.Q.S. Le, C.E. Bünger, In situ synthesis of three dimensional graphene/hydroxyapatite nano powders via hydrothermal process, Mater. Chem. Phys. 222 (2019) 251–255, http://dx.doi.org/10.1016/j.matchemphys.2018.10.023.
[40] M. Landin, R.C. Rowe, P. York, Structural changes during the dehydration of dicalcium phosphate dihydrate, Eur. J. Pharmac. Sci. 2 (1994) 245–252, http://dx.doi.org/10.1016/0928-0987(94)90029-9.
[41] W.C. Chen, K.C. Chang, H.Y. Wu, C.L. Ko, C.L. Huang, Thermal cycling effect of dicalcium phosphate-reinforced composites on auto-mineralized dental resin, Mater. Sci. Eng. C 45 (2014) 359–368, http://dx.doi.org/10.1016/j.msec.2014.09.032.
[42] H. Nosrati, R. Sarraf Mamoory, F. Dabir, D.Q.S. Le, C.E. Bünger, M.C. Perez, M.A. Rodriguez, Effects of hydrothermal pressure on in situ synthesis of 3D graphene/hydroxyapatite nano structured powders, Ceram. Int. 45 (2019) 1761–1769, http://dx.doi.org/10.1016/j.ceramint.2018.10.059.
[43] H. Shi, J. Zhang, X. Ye, T. Wu, T. Yu, J. Ye, Formation and stability of well-crystallized metastable octacalcium phosphate at high temperature by regulating the reaction environment with carbamide, CrystEngComm 21 (2019) 5174–5184, http://dx.doi.org/10.1039/c9ce00677j.
[44] H. Nosrati, R. Sarraf-Mamoory, D.Q.S. Le, C.E. Bunger, Preparation of reduced graphene oxide/hydroxyapatite nanocomposite and evaluation of graphene sheets/hydroxyapatite interface, Diamond Relat. Mater. 100 (2019) 107561, http://dx.doi.org/10.1016/j.diamond.2019.107561.
[45] T.K. Anee, N.M. Sundaram, D. Arivuoli, P. Ramasamy, S.N. Kalkura, Influence of an organic and an inorganic additive on the crystallization of dicalcium phosphate dihydrate, J. Crystal Growth 285 (2005) 380–387, http://dx.doi.org/10.1016/j.jcrysgro.2005.08.036.
[46] Y. Su, Y. Guo, Z. Huang, Z. Zhang, G. Li, J. Lian, L. Ren, Preparation and corrosion behaviors of calcium phosphate conversioncoating on magnesium alloy, Surf. Coat. Technol. 307 (2016) 99–108, http://dx.doi.org/10.1016/j.surfcoat.2016.08.065.
[47] C. Combes, C. Rey, M. Freche, XPS and IR study of dicalcium phosphate dihydrate nucleation ontitanium surfaces, Colloids Surf. B: Biointerfaces 11 (1998) 15–27, http://dx.doi.org/10.1016/S0927-7765(98)00014-9.
[48] A.M. Yousefi, A review of calcium phosphate cements and acrylic bone cements as injectable materials for bone repair and implant fixation, J. Appl. Biomater. Funct. Mater. 17 (4) (2019) 1–21, http://dx.doi.org/10.1177/2280800019872594.
[49] M.H. Esnaashary, H.R. Rezaie, A. Khavandi, J. Javadpour, Evaluation of setting time and compressive strength of a new bone cement precursor powder containing Mg–Na–Ca, J. Eng. Med. 232 (10) (2018) 1017–1024, http://dx.doi.org/10.1177/0954411918796048.
[50] E. Şahin, Calcium Phosphate Bone Cements, Intechopen, doi:10.5772/intechopen.74607.